The Journal of Chemical Physics

RESEARCH ARTICLE | NOVEMBER 01 2023

Electrochemical AFM/STM with a qPlus sensor: A versatile tool to study solid-liquid interfaces

Special Collection: 2023 JCP Emerging Investigators Special Collection

Andrea Auer ; Bernhard Eder ; Franz J. Giessibl

J. Chem. Phys. 159, 174201 (2023)
https://doi.org/10.1063/5.0168329

AIP Publishing

The Journal of Chemical Physics ARTICLE pubs.aip.org/aip/jcp

Electrochemical AFM/STM with a qPlus sensor: A versatile tool to study solid-liquid interfaces

Cite as: J. Chem. Phys. 159, 174201 (2023); doi: 10.1063/5.0168329
Submitted: 18 July 2023 • Accepted: 29 August 2023 •
Published Online: 1 November 2023

Andrea Auer,[a] Bernhard Eder, and Franz J. Giessibl

AFFILIATIONS

Institute of Experimental and Applied Physics, University of Regensburg, 93053 Regensburg, Germany

Note: This paper is part of the 2023 JCP Emerging Investigators Special Collection.
[a]**Author to whom correspondence should be addressed:** andrea.auer@ur.de

ABSTRACT

Atomic force microscopy (AFM) that can be simultaneously performed with scanning tunneling microscopy (STM) using metallic tips attached to self-sensing quartz cantilevers (qPlus sensors) has advanced the field of surface science by allowing for unprecedented spatial resolution under ultrahigh vacuum conditions. Performing simultaneous AFM and STM with atomic resolution in an electrochemical cell offers new possibilities to locally image both the vertical layering of the interfacial water and the lateral structure of the electrochemical interfaces. Here, a combined AFM/STM instrument realized with a qPlus sensor and a home-built potentiostat for electrochemical applications is presented. We demonstrate its potential by simultaneously imaging graphite with atomic resolution in acidic electrolytes. Additionally, we show its capability to precisely measure the interfacial solvent layering along the surface normal as a function of the applied potential.

I. INTRODUCTION

In electrochemistry there is a highly complex interplay between the reactants, solvent molecules, and the electrode surface. Therefore, it is necessary to systematically unravel these effects by employing fundamental model studies. The electrochemical interface is not only governed by the nature of the electrode material but also by the electrochemical double layer structure, which includes the distinct structure of the electrolyte solution.[1] Spatially-resolved imaging at the atomic scale of these structures is therefore at the core of both fundamental electrochemistry research and future application. While the development of *in situ* characterization tools, such as spectroscopy[2–8] and scanning probe microscopy approaches,[9–13] in combination with theoretical simulations[14–17] has strongly advanced our knowledge of the interfacial structure, e.g., by revealing structural properties of the electrode surface and ion adsorbate layers, the precise characterization of the local interfacial solvent structure as well as the water and ion densities remains extremely challenging and largely inaccessible. In contrast to *in situ* applications mostly used to determine the electrode structure and morphology in an electrochemical environment, AFM-based methods have been employed to image the interface and in particular the hydration structures, i.e., the layered arrangement of the interfacial water molecules formed at crystalline mineral surfaces, see e.g., Refs. 18–23. Visualizing the interfacial organization and the preferential alignment of water molecules and ions as well as the surface structure at the electrochemical double layer under variable potential control using combined AFM/STM is a new experimental approach to directly image the entire electrified solid/liquid interface in a single measurement. Microscopes that allow for both atomically-resolved atomic force microscopy (AFM) and scanning tunneling microscopy (STM) and seamless transitions in between, have become easily realizable by using self-sensing quartz cantilevers (qPlus sensors).[24] Simultaneous AFM/STM experiments using the qPlus sensor have strongly advanced high precision measurements of surfaces under ultrahigh vacuum conditions,[25,26] even reaching unprecedented subatomic spatial resolution.[24,27,28]

The use of frequency-modulation AFM (FM-AFM) performed with stiff qPlus sensors has led to significant advances in measuring and interpreting high-resolution AFM images as well as force-distance curves in both ambient[22,24,29,30] and liquid environments.[31,32] It was further demonstrated that it is possible to image soft biological samples in liquid using a qPlus setup and atomic resolution on mica was achieved in a variety of liquids.[30] The stiffness of the sensors allows the use of very small amplitudes in frequency-modulation detection mode, which consequently means a high sensitivity to short-range forces is obtained,[24] and that images can be acquired with no or little downward force, thus prevent-

ing unwanted destruction or deformation of the soft double-layer structures. Exploitation of the advantages of the qPlus sensor and its application to the field of electrochemistry enables the direct observation of the complex interfacial organization of solvent molecules at electrochemical solid/liquid interfaces and the corresponding lateral structure of the electrode under electrochemical conditions.

In this work, we present an electrochemical AFM/STM system based on a qPlus sensor with a home-built potentiostat design that makes use of an external electronic control unit. This electronic control unit acts as a power supply, analog output, analog-to-digital converter, and function generator. For these external components, we utilize the Nanonis™ (SPECS Zurich GmBH, Switzerland) microscope control system. We include a detailed description of the experimental setup and discuss the requirements to perform simultaneous *in situ* EC-AFM/STM measurements with potential control in an operating electrochemical cell. We present atomically resolved simultaneous AFM and STM images of the electrode surface. Finally, we show potential-dependent 2D frequency shift vs distance maps to reveal the vertical and lateral interfacial solvent structure at a HOPG interface in aqueous sulfuric acid (H_2SO_4) over a wide potential range.

II. A QPLUS SENSOR SETUP FOR ELECTROCHEMICAL MEASUREMENTS

To realize an electrochemical qPlus sensor-based setup, which allows simultaneously AFM and STM measurements, a home-built scanning probe microscope,[30] was adapted with a home-built potentiostat to allow for variable potential control (see Sec. III). As illustrated in Fig. 1(a), our EC-AFM/STM setup consists of several components, namely a qPlus sensor, a long and sharp tip and a three-electrode electrochemical cell connected to a potentiostat.

A. Electrochemical cell

The three-electrode electrochemical cell [Figs. 1(a) and 1(b)] is based on a typical *in situ* SPM cell and is made of Teflon. The top part has small drill holes in it to fix both the counter electrode (CE) and a quasi-reference electrode (RE), here e.g., Pt/Ir wires. These electrodes are connected to the potentiostat as shown in Fig. 2(a). The potential of the quasi-RE was determined to be −0.8 V vs the standard hydrogen electrode (SHE) using the voltammetric response of a Au(111) single crystal in 0.1M H_2SO_4, which is in excellent agreement with the potential of a Pt wire as determined in literature.[33]

B. qPlus sensors and tip materials

For the electrochemical setup to simultaneously measure AFM and STM *in situ*, a qPlus sensor of the third generation (Type S0.6)[24] with a high stiffness factor k = 9400 N/m was used, which leads to a resonance frequency of around 30 kHz with the attached tip. The sensor has three gold electrodes for the AFM and STM signals [see Fig. 1(a)]. The upper/lower and side electrodes serve for the differential detection of the deflection of the beam and are connected to the AFM preamplifier.[30] The center electrode is employed to bias the tip for STM operation and is conductively connected to a metallic tip. The application of a bias voltage as well as the measurement of the tunneling current is achieved by a combination of a transimpedance amplifier and a difference amplifier.[30] As mentioned, the bias is applied to the tip and thus the sample is grounded. In the electrochemical setup, however, the electrochemical electrode potential of the sample can be varied with respect to a reference electrode (RE). Therefore, the bias voltage is the difference of the potential applied to the tip and to the sample:

$$U_{\text{bias}} = E_{\text{tip}} - E_{\text{sample}} \tag{1}$$

Usually in an EC-SPM setup, the bias voltage is applied to the sample, which then requires the use of a so-called bipotentiostat, where the tip potential can be varied independently of the working electrode potential both with respect to the RE and the bias is given analogously by Eq. (1).[11]

A relatively long tip, which can consist of a variety of different tip materials, was glued onto the prong of the qPlus sensor. While these long tips decrease both the quality factor and free resonance frequency of our qPlus sensors,[34] they are found to not strongly affect the normal force measurements.[35] We recently considered both theoretically and experimentally the lateral motion of our long tips and concluded that the lateral motion can be neglected.[34] Note that the length of the tip (here ~3 mm, see also Fig. S1) is dependent on the thickness of the top part of the electrochemical cell, where it must be assured that the qPlus sensor with its open gold electrodes[24] does not contact the electrolyte solution. For simultaneous AFM/STM measurements the tip needs to be metallic to be able to measure the tunneling current. Therefore, in this study, electrochemically etched platinum-iridium (Pt/Ir) tips, which are subsequently coated with Apiezon wax [Figs. S1(a) and S1(b)], are employed, analogous to tips commonly-used for EC-STM measurements.[11] To confirm the general quality of the coating, an exemplary z-spectroscopy measurement (tunneling current vs relative z-distance) is shown in Fig. S2, where a low leakage current of <30 pA was obtained for a coated Pt/Ir tip at E_{tip} = 0.35 V_{SHE}. While the tunneling current shows the expected short-range exponential decay decreasing to the leakage current at a relative z value of 0.5 nm, the simultaneously recorded Δf spectrum has a much different distance dependence, showing a clear signal at distances over 1 nm. This difference unambiguously shows that this EC microscope setup can measure two independent channels (tunneling current as well as frequency shift). The qPlus sensor is highly flexible and can be mounted with a variety of different tip materials. Since it has been previously shown that silicon (Si) cantilevers are well suited for the imaging of hydration structures,[18] the qPlus sensors used in this study were additionally equipped with a Si splinter that was extended with a tungsten wire to reach the necessary length of around 3 mm [see Fig. S1(c)] for only AFM measurements. Exemplary frequency sweep curves for the same sensor in air and with the tip immersed in solution are shown in Fig. 1(c) (amplitude vs frequency shift) and d (phase vs frequency shift). Immersion of the tip leads to a decrease in both resonance frequency (a few 100 Hz) and the Q value (from around 3600 to 230).

C. Home-built potentiostat design

A potentiostat is essential for any EC-SPM setup. It allows the interfacial potential of the working electrode, i.e., the sample that is to be investigated, to be accurately controlled in a three-electrode electrochemical cell. Here a simple electric circuit [adapted from

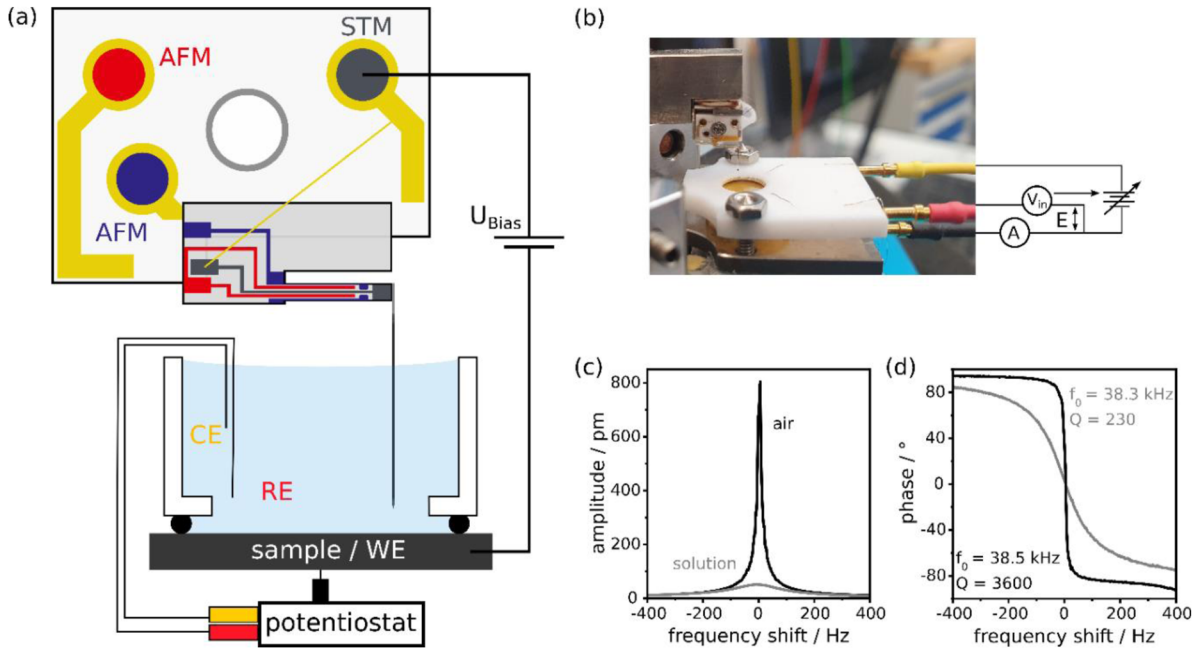

FIG. 1. Schematic illustration (a) and photograph (b) of the electrochemical qPlus sensor-based AFM/STM setup with its three-electrode configuration electrochemical cell. Frequency sweep curves for the same sensor in air and while the tip is immersed in solution. (c) Amplitude and (d) phase vs frequency shift.

Ref. 36, see Fig. 2(a)] is presented based on three operational amplifiers (op-amp, *LF356*, Texas Instruments, Inc. USA), which enables potentiostatic control as well as the measurement of electrochemical currents at the sample electrode. To control the potential of the working electrode, a voltage (V_{in}) is applied to the CE, which provides enough current to compensate for any redox reactions occurring at the WE. The applied potential is regulated by a feedback loop from the RE.

The DC power supply of the Nanonis control unit of our microscope (±15 V) is used to power all three LF356 with a DC voltage. Although the LF356 operational amplifiers can have a maximum power supply voltage of ±18 V, we included a voltage regulator (Fig. S3) from ±15 to ±5 V, which additionally acts as a low pass filter to reduce the noise of the power supply voltage. Note that the voltage reduction is not necessary for the combination of the Nanonis supply and these op-amps, and it will reduce the output voltage of the current follower, i.e., the current range (see below). The control signal is applied through two summing resistors (R_1 = 15 kΩ) to the first op-amp with its output connected to the CE, which then provides current to compensate for the voltage drop across R_c (iR_C), the compensated cell resistance. The RE is configured in a negative feedback loop, where a unity gain buffer, our second op-amp, prevents current flow through the RE.[36] As illustrated in Fig. 2(a), the electrochemical cell in a three-electrode configuration can be modelled by two resistors in series,[36] which represent a compensated and an uncompensated cell resistance between CE and RE (R_c) and between RE and WE (R_u), respectively. While R_c can be compensated by the input control signal, R_u can only be minimized by positioning the RE close to the WE. To be able to measure Faradaic currents that can occur due to electrochemical redox reactions at the WE, a third op-amp, here a transimpedance amplifier with a feedback resistor R_2 = 20 kΩ, is used. The third op-amp converts the current to a potential V_{out} with a 5 V voltage supply, a maximum current of 250 μA can be measured. While the analog circuitry is rather simple, the potentiostat requires the Nanonis control unit to control the potentials as well as to record the input and output signals. This furthermore allows us to use the sweep function of the Nanonis setup to modulate the control signal as a function of time and perform cyclic voltammetry measurements without the need of an additional function generator. Calibration measurements and the corresponding U-I characteristics of various resistors and a RC-circuit (with R = 1 kΩ and C = 1 mF) are shown in Fig. 2(b). The potentiostat was additionally tested on a well-defined model system, gold (Au) in 0.1M H_2SO_4, where the characteristic oxidation and reduction peaks, shown in Fig. 2(c), were used to determine the potential of the Pt/Ir pseudo-reference electrode ($E_{SHE} = E_{Pt/Ir} + 0.8$ V).

III. EXPERIMENTAL DETAILS

Prior to all measurements, the Teflon cell including the electrode wires was cleaned in freshly prepared piranha acid (3:1, H_2SO_4:H_2O_2) and boiled in ultrapure water (Thermofisher purification system, >18 MΩ cm) to remove (organic) contaminants. The qPlus sensor (Type S0.6) was assembled on an aluminum oxide substrate and the respective STM and AFM electrodes were connected using conductive epoxy (EPO-TEK H20E) and, if necessary, a thin Au wire. Two types of tips were used: A conducting Pt/Ir wire

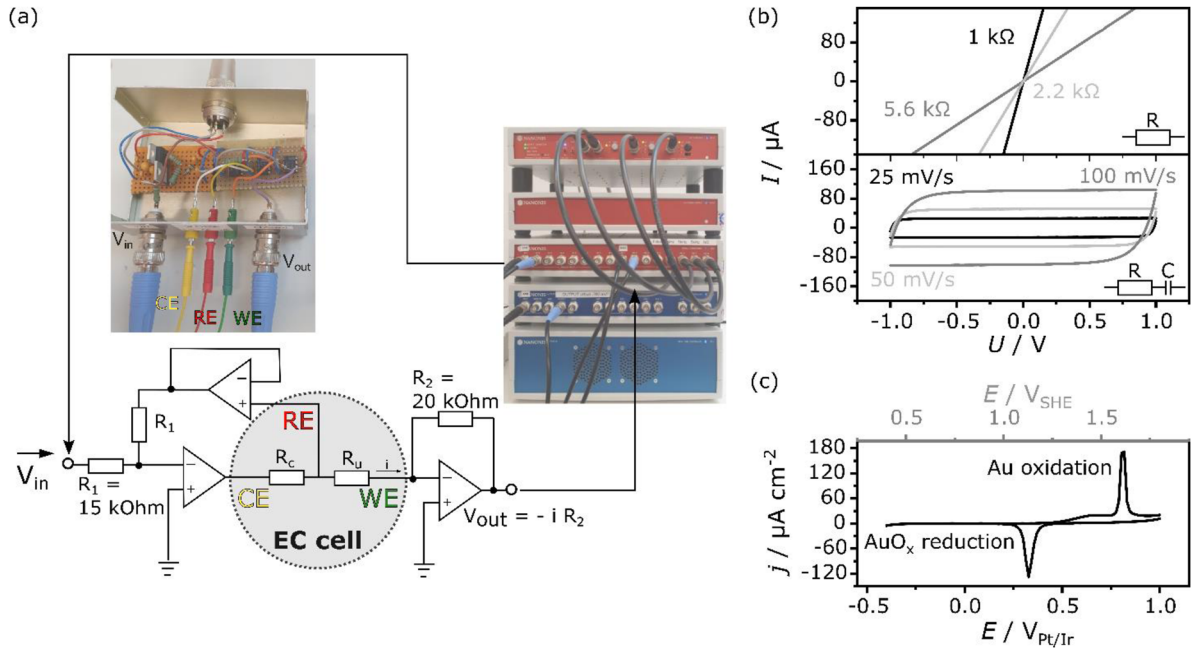

FIG. 2. Electric circuit of the home-built potentiostat design. (a) Electrochemical (EC) cell and the corresponding potentiostatic control circuit utilizing the Nanonis^{TM} control-unit of our microscope. RE stands for reference electrode, CE for counter electrode and WE for working electrode. The inset shows the assembled potentiostat board. (b) U-I characteristics of different resistors and a RC circuit (R = 1 kΩ, C = 1 mF). (c) Cyclic voltammogram of a Au(111) single crystal in 0.1M H_2SO_4 measured in the *in situ* cell using the home-built potentiostat.

for simultaneous AFM/STM imaging (Fig. 3) and a W wire with a Si splinter for AFM and the 2D frequency shift vs distance maps (Fig. 4). The latter allows us to be comparable to previous AFM studies on water structures near surfaces, e.g., Refs. 18–21 and 37, where commonly soft Si cantilevers are used. The metal wire diameter in both cases was 50 μm and was attached to the beam of the qPlus sensor. The Pt/Ir tip was electrochemically etched in an aqueous 2M KOH/4M KSCN (Merck, EMSURE) solution on the qPlus sensor utilizing a tantalum (Ta) ring electrode as the counter electrode. Between the Pt/Ir wire and the Ta electrode an AC voltage of 10 V (peak-to-peak) with a frequency of 1 kHz and a DC offset of 2 V was applied, similar to the procedure described in Refs. 11 and 38. The tip was degreased in an acetone/water mixture and thoroughly rinsed in ultrapure water prior to subsequent coating with Apiezon wax. Representative micrographs of the tips are shown in Fig. S1. The 0.1M H_2SO_4 electrolyte solution used for all measurements presented in this work was prepared from H_2SO_4 (96%, Merck, Suprapur) and ultrapure water.

The 2D frequency shift vs distance maps are measured as follows: First, the oscillation amplitude is set to a small value of around 50–90 pm, which results in a peak-to-peak amplitude smaller than the diameter of the solvent molecules. The distance of the tip apex to the surface is regulated by a set Δf value. Then the AFM tip is vertically retracted and approached a set value (nominally 5 nm) from and to the surface [relative z direction (z_{rel})] with an open feedback loop. The Δf feedback is enabled after every approach, and the tip is laterally moved to the next preset x-offset value adjusting to the Δf value. This allows us to measure 1D frequency shift spectra over a line scan (here 4.3 nm) with a defined step size (here 0.14 nm), which results in 30 single spectra for each line scan. The frequency shift vs distance spectra for the different potentials were recorded sequentially: The potential was set to a value in the middle of the double layer region (i.e., around 0.8 V_{SHE}) prior to subsequent potential steps to more negative and positive values ($\Delta E = 200$ mV). To ensure steady state conditions, we waited ~5 min before measuring at each potential. For the potential-dependent analysis of the layer distance, 6 datasets, i.e., line scans at different positions on the sample at the same potential, measured with two different Si tips were evaluated. To minimize noise and allow for a more accurate evaluation, the average curve from the line scan was used for the determination of the layer distances. After excluding non-meaningful single spectra that showed no oscillations, each data point includes 130 to 180 single spectra.

IV. RESULTS AND DISCUSSION

A. Simultaneous AFM/STM measurements

Atomically resolved simultaneous AFM and STM measurements were performed on a HOPG electrode in 0.1M H_2SO_4 solution at E = 0.85 V_{SHE}. Figure 3 shows both large area AFM and STM images of the HOPG surfaces as well as high-resolution images of the channels of interest, i.e., the topographic (z), the frequency shift (Δf) and the tunneling current channel. The overview images [Figs. 3(a)–3(c)] taken in AFM feedback with an applied bias of −500 mV show large terraces of the HOPG surfaces separated by

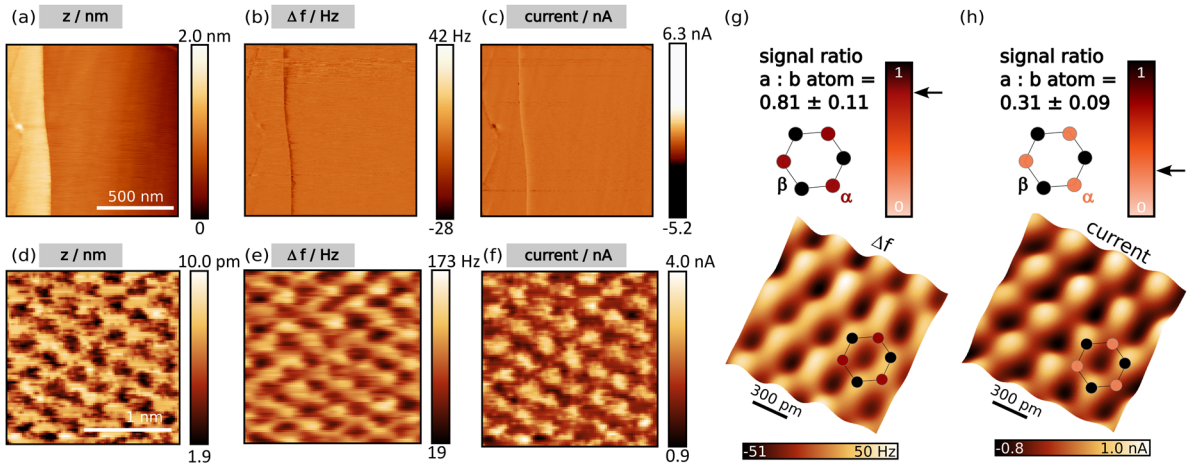

FIG. 3. Simultaneous electrochemical AFM/STM images of a freshly cleaved HOPG surface in 0.1M H_2SO_4 at a potential E = 0.85 V_{SHE}. Large scan area images [$(1 \times 1)\ \mu m^2$] showing the morphology of the electrode surface in the (a) topographic (z), (b) Δf and (c) current channel. E_{tip} = 0.35 V_{SHE}, Bias = −500 mV, Amplitude = 250 pm. (d)–(f) Atomically resolved images [$(2.5 \times 2.5)\ nm^2$] taken in quasi-constant height mode with an amplitude of 50 pm. (g)–(h) Evaluated signal contrast of the α and β atom with respect to the hollow site [n = 9, measured at all three α (β) sites of different hexagons] to show the difference in contrast in a quantitative way and reconstructed images by inverse 2D fast Fourier transformation (Fig. S5) of the frequency shift and tunneling current images. The α and β atom are colored according to their signal ratio.

a step. Additional images taken in STM feedback, while simultaneously recording the Δf channel, are shown in Fig. S4. The contrast of the morphology of the surface is clearly visible in all channels.

Atomic resolution is shown in Figs. 3(d)–3(f). These images were taken in quasi-constant height mode, which means that the Δf feedback is reduced so that the tip roughly follows the surface topography. While ideally one would perform constant-height imaging, where the z-control is turned off, this is often challenging at room temperature due to thermal drift. Thus, low contrast can be observed in the topographic image. Atomic contrast can be seen in the frequency shift and current channels, where distinct differences are observed. While in the Δf image the honeycomb lattice [Fig. 3(g)] of the graphite surface is visible, in the current image a triangular structure is observed [Fig. 3(h)]. In the STM image, only every second atom, the β atom, of the hexagonal lattice is visible due to the different electronic structure of the neighboring carbon atoms.[39,40] Similar to previous measurements under UHV conditions in a low-temperature microscope,[41] we show that AFM can resolve both the α and β atom of the graphite structure as a result of the total charge interaction with the tip under electrochemical conditions. To quantify the observed difference in contrast, the signal ratio between the α and β atom with respect to the hollow site is given in Figs. 3(g) and 3(h). First the signal intensity over the α and β sites is determined, which is the difference between the signal at the α (or β) site and the minimal value of the signal (occurring at the center of the hexagons). Then the signal ratio α: β is determined, which is the ratio between the signal intensity of the α site and the signal intensity of β site. While the α atom appears at a similar intensity as the β atom in the Δf image (α: β = 0.81 ± 0.11), it appears at a lower intensity in the current image (α: β = 0.31 ± 0.09). This shows that there is a clear difference in contrast in the AFM and STM channel, in good agreement with previous literature.[41]

B. Potential-dependent interfacial water organization

AFM based methods, in contrast to STM, are not only able to resolve the lateral structure of an electrode surface, but can also access the structure of solvent molecules, i.e., water and ion densities, along the surface normal.[18,42] Previous work by Utsunomiya *et al.* reported potential-dependent solvent structures at the HOPG/aqueous electrolyte, where the oscillatory modulations in single 1D force spectra were correlated to a layered distribution of interfacial water (i.e., hydration layers).[37] Interestingly, they observed an oscillation wavelength slightly decreasing from 0.4 to 0.3 nm with increasing potential. The layer-to-layer distance agrees with the expected thickness of a single water layer as well as with measurements in pure water without external potential control.[43,44] Additionally to anion-dependent hydration properties of the graphite electrode with an apparent stabilizing effect of sulfate (SO_4^{2-}) compared to perchlorate (ClO_4^-) ions, the authors found an increased modulation length of structured liquid for anodic (positive) potentials.[37]

We performed repeated frequency shift vs distance measurements with a lateral offset (x-offset) between each measurement to resolve the interfacial molecular organization of the liquid at the electrochemical interface (see Fig. 4). Figure 4 shows 2D plots and the corresponding average frequency shift vs distance curves over a wide range of applied potentials at the HOPG/H_2SO_4 interface. These 2D measurements allow us to gather information about both the vertical and lateral arrangement of the previously reported potential dependent hydration structures. Indeed, we observe clear frequency shift oscillations [represented by the bright bands in the 2D plots (a)–(c)], where the number, strength, and the wavelength of the oscillations, which we denote as the "layer distance", are dependent on the applied potential. The reversibility of these

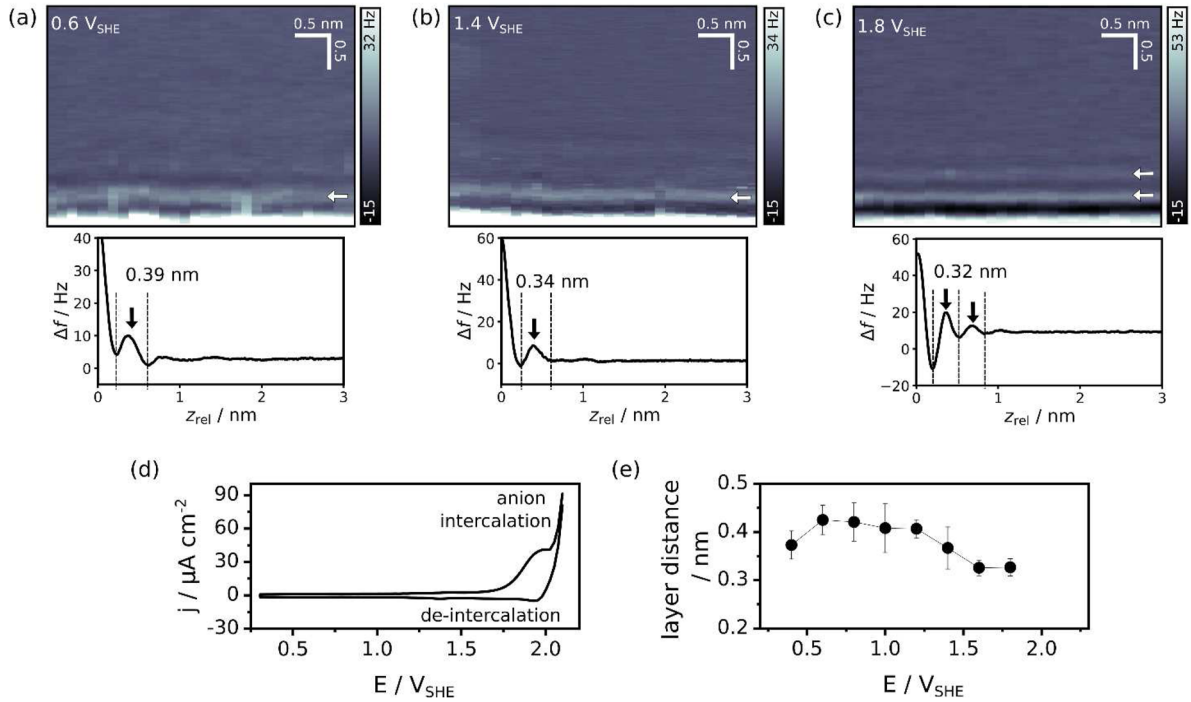

FIG. 4. (a)–(c) 2D frequency shift vs distance maps and corresponding average curves for the shown line scan at different potentials along the surface normal of a HOPG surface in a 0.1M H_2SO_4 electrolyte. (d) Cyclic voltammogram of HOPG in 0.1M H_2SO_4 and (e) the corresponding, average layer distances as a function of the measured potential. The error bars correspond to the standard error of the average for 6 data sets taken with two different tips.

potential-dependent changes in solvent structure is illustrated by comparing average frequency shift vs distance curves at 1.8 V_{SHE} before and after measuring at the lowest applied potential of 0.4 V_{SHE} (see Fig. S6). Identical features and the same layer distances are observed, demonstrating reversible changes in the solution structure upon a change in potential.[37] Similar to previous reports at the HOPG/water interface with no externally applied potential,[43,44] the 2D plots show no lateral structure independent of the applied potential and only vertical layering is observed. Figure 4(d) displays the CV of HOPG in 0.1M H_2SO_4 taken in the *in situ* SPM electrochemical cell. The corresponding average values for the layer distances at each measured potential are shown in Fig. 4(e). The Δf modulation shows a small decrease in layer distance from ~0.4 nm (E = 0.4 to 1.2 V_{SHE}) to 0.3 nm (E = 1.5–1.8 V_{SHE}), which has been previously observed in literature.[37] The vertical layer distance of 0.3–0.4 nm is in good agreement with the expected thickness of a water layer, suggesting that the overall electrolyte structure is dominated by water over the whole applied potential range. In addition to the small decrease in layer distance, the number of observed layers increases at high anodic potentials. We attribute both to a more compact and pronounced structuring of water due to the increased interfacial charge and/or a stabilizing effect of the (adsorbed) sulfate ions.[37] To unravel the precise role of electrode material, applied potential and ions on the interfacial solvent structure, further systematic studies are needed.

V. CONCLUSION

In this work, we have presented an electrochemical qPlus sensor-based SPM setup with a home-built potentiostat including a detailed description of the experimental requirements and details. Atomic resolution of graphite was obtained in both AFM and STM channels in an electrolyte solution with an externally applied potential, demonstrating that simultaneous measurements are possible in an ambient, electrochemical qPlus-based SPM setup using comparably long tips. The observed difference in contrast between the AFM and STM images of a HOPG surface demonstrates the capability to measure conductance at the Fermi level (STM) as well as the total charge density (AFM) in an electrolyte solution. This means that this setup has the potential to resolve electrode surface processes that are accompanied by a change in charge density, i.e., adsorption, intercalation, or oxidation processes, and their atomic contrasts in greater detail.

FM-AFM and 2D frequency shift vs distance maps were used to measure the vertical and lateral molecular solvent structure. The structure exhibits only a vertical layer arrangement with a modulation of 0.3–0.4 nm, which suggests that the overall solvent structure is dominated by water layers. These results are congruent with the previous literature,[37] demonstrating the accuracy, reproducibility and sensitivity of the EC-AFM setup based on very stiff qPlus sensors for evaluating molecular-scale structures at the solid-liquid

interface. Our results show the versatility of a qPlus sensor-based combined EC-AFM/STM setup and how new imaging approaches can help to gain a fundamental understanding of electrochemical interfaces with spatial resolution including the atomic/molecular structures of both the electrode and the electrolyte.

SUPPLEMENTARY MATERIAL

Please see supplementary material for detailed photo- and micrographs of the qPlus 0.6 sensor and the attached tips; simultaneous z-spectroscopy measurements; the electric circuit of the voltage regulator down to ±5 V to supply the op-amps of the potentiostat; additional topographic images in STM feedback; 2D Fast Fourier transformation of the images shown in Figs. 3(e) and (f); additional frequency vs distance curves to show reversibility of the potential-dependent changes.

ACKNOWLEDGMENTS

A.A. gratefully acknowledges funding from the Alexander von Humboldt Foundation via the Research Fellowship Program. We thank Alfred J. Weymouth for fruitful discussions and proofreading. A.A. thanks Theresa Seeholzer for initial training on the microscope.

AUTHOR DECLARATIONS

Conflict of Interest

F.J.G. holds patents about the force sensors used in the experiments. The remaining authors declare no competing interests.

Author Contributions

Andrea Auer: Conceptualization (equal); Funding acquisition (equal); Investigation (lead); Methodology (lead); Project administration (equal); Visualization (equal); Writing – original draft (equal); Writing – review & editing (equal). **Bernhard Eder**: Investigation (supporting); Visualization (supporting); Writing – review & editing (supporting). **Franz J. Giessibl**: Conceptualization (equal); Methodology (supporting); Resources (equal); Writing – review & editing (equal).

DATA AVAILABILITY

The data that support the findings of this study are available within the article and its supplementary material.

REFERENCES

[1]M. T. M. Koper, "Thermodynamic theory of multi-electron transfer reactions: Implications for electrocatalysis," J. Electroanal. Chem. **660**(2), 254–260 (2011).
[2]M. F. Toney, J. N. Howard, J. Richer, G. L. Borges, J. G. Gordon, O. R. Melroy, D. G. Wiesler, D. Yee, and L. B. Sorensen, "Voltage-dependent ordering of water molecules at an electrode–electrolyte interface," Nature **368**(6470), 444–446 (1994).
[3]K. I. Ataka, T. Yotsuyanagi, and M. Osawa, "Potential-dependent reorientation of water molecules at an electrode/electrolyte interface studied by surface-enhanced infrared absorption spectroscopy," J. Phys. Chem. **100**(25), 10664–10672 (1996).
[4]A. Foelske-Schmitz, in *Encyclopedia of Interfacial Chemistry*, edited by K. Wandelt (Elsevier, 2018), pp. 591–606.
[5]F. Zaera, "Probing liquid/solid interfaces at the molecular level," Chem. Rev. **112**, 2920–2986 (2012).
[6]M. Favaro, B. Jeong, P. N. Ross, J. Yano, Z. Hussain, Z. Liu, and E. J. Crumlin, "Unravelling the electrochemical double layer by direct probing of the solid/liquid interface," Nat. Commun. **7**(1), 12695 (2016).
[7]O. M. Magnussen and A. Groß, "Toward an atomic-scale understanding of electrochemical interface structure and dynamics," J. Am. Chem. Soc. **141**(12), 4777–4790 (2019).
[8]J. J. Velasco-Velez, C. H. Wu, T. A. Pascal, L. F. Wan, J. Guo, D. Prendergast, and M. Salmeron, "The structure of interfacial water on gold electrodes studied by x-ray absorption spectroscopy," Science **346**(6211), 831–834 (2014).
[9]K. Itaya and E. Tomita, "Scanning tunneling microscope for electrochemistry - a new concept for the in situ scanning tunneling microscope in electrolyte solutions," Surf. Sci. **201**(3), L507 (1988).
[10]A. A. Gewirth and B. K. Niece, "Electrochemical applications of in situ scanning probe microscopy," Chem. Rev. **97**(4), 1129–1162 (1997).
[11]M. Nowicki and K. Wandelt, *Encyclopedia of Interfacial Chemistry* (Elsevier, 2018), pp. 108–128.
[12]Y. Liang, J. H. K. Pfisterer, D. McLaughlin, C. Csoklich, L. Seidl, A. S. Bandarenka, and O. Schneider, "Electrochemical scanning probe microscopies in electrocatalysis," Small Methods **3**, 1800387 (2019).
[13]L. A. Kibler and D. M. Kolb, in *Handbook of Fuel Cells*, edited by W. Vielstich, H. A. Gasteiger, A. Lamm, and H. Yokokawa (John Wiley & Sons, Ltd., 2010), pp. 1–13.
[14]J. Rossmeisl, E. Skúlason, M. E. Björketun, V. Tripkovic, and J. K. Nørskov, "Modeling the electrified solid-liquid interface," Chem. Phys. Lett. **466**(1–3), 68–71 (2008).
[15]A. Groß, *Surface and Interface Science* (Wiley, 2020), pp. 471–515.
[16]N. G. Hörmann, O. Andreussi, and N. Marzari, "Grand canonical simulations of electrochemical interfaces in implicit solvation models," J. Chem. Phys. **150**(4), 041730 (2019).
[17]H. H. Heenen, J. A. Gauthier, H. H. Kristoffersen, T. Ludwig, and K. Chan, "Solvation at metal/water interfaces: An *ab initio* molecular dynamics benchmark of common computational approaches," J. Chem. Phys. **152**(14), 144703 (2020).
[18]T. Fukuma and R. Garcia, "Atomic- and molecular-resolution mapping of solid-liquid interfaces by 3D atomic force microscopy," ACS Nano **12**(12), 11785–11797 (2018).
[19]T. Fukuma, Y. Ueda, S. Yoshioka, and H. Asakawa, "Atomic-scale distribution of water molecules at the mica-water interface visualized by three-dimensional scanning force microscopy," Phys. Rev. Lett. **104**(1), 016101 (2010).
[20]K. Kimura, S. Ido, N. Oyabu, K. Kobayashi, Y. Hirata, T. Imai, and H. Yamada, "Visualizing water molecule distribution by atomic force microscopy," J. Chem. Phys. **132**(19), 194705 (2010).
[21]H. Söngen, M. Nalbach, H. Adam, and A. Kühnle, "Three-dimensional atomic force microscopy mapping at the solid-liquid interface with fast and flexible data acquisition," Rev. Sci. Instrum. **87**(6), 063704 (2016).
[22]D. S. Wastl, M. Judmann, A. J. Weymouth, and F. J. Giessibl, "Atomic resolution of calcium and oxygen sublattices of calcite in ambient conditions by atomic force microscopy using qPlus sensors with sapphire tips," ACS Nano **9**(4), 3858–3865 (2015).
[23]E. Wutscher and F. J. Giessibl, "Atomic force microscopy at ambient and liquid conditions with stiff sensors and small amplitudes," Rev. Sci. Instrum. **82**(9), 093703 (2011).
[24]F. J. Giessibl, "The qPlus sensor, a powerful core for the atomic force microscope," Rev. Sci. Instrum. **90**(1), 011101 (2019).
[25]F. Stilp, A. Bereczuk, J. Berwanger, N. Mundigl, K. Richter, and F. J. Giessibl, "Very weak bonds to artificial atoms formed by quantum corrals," Science **372**(6547), 1196–1200 (2021).
[26]F. Giessibl, "Probing the nature of chemical bonds by atomic force microscopy," Molecules **26**(13), 4068 (2021).

[27]M. Emmrich, F. Huber, F. Pielmeier, J. Welker, T. Hofmann, M. Schneiderbauer, D. Meuer, S. Polesya, S. Mankovsky, D. Ködderitzsch, H. Ebert, and F. J. Giessibl, "Subatomic resolution force microscopy reveals internal structure and adsorption sites of small iron clusters," Science **348**(6232), 308–311 (2015).
[28]F. Huber, J. Berwanger, S. Polesya, S. Mankovsky, H. Ebert, and F. J. Giessibl, "Chemical bond formation showing a transition from physisorption to chemisorption," Science **366**(6462), 235–238 (2019).
[29]D. S. Wastl, A. J. Weymouth, and F. J. Giessibl, "Optimizing atomic resolution of force microscopy in ambient conditions," Phys. Rev. B **87**(24), 245415 (2013).
[30]K. Pürckhauer, S. Maier, A. Merkel, D. Kirpal, and F. J. Giessibl, "Combined atomic force microscope and scanning tunneling microscope with high optical access achieving atomic resolution in ambient conditions," Rev. Sci. Instrum. **91**(8), 083701 (2020).
[31]K. Pürckhauer, A. J. Weymouth, K. Pfeffer, L. Kullmann, E. Mulvihill, M. P. Krahn, D. J. Müller, and F. J. Giessibl, "Imaging in biologically-relevant environments with AFM using stiff qPlus sensors," Sci. Rep. **8**(1), 9330 (2018).
[32]A. J Weymouth, D. Wastl, and F. J Giessibl, "Advances in AFM: Seeing atoms in ambient conditions," e-J. Surf. Sci. Nanotechnol. **16**, 351–355 (2018).
[33]K. K. Kasem and S. Jones, "Platinum as a reference electrode in electrochemical measurements," Platinum Met. Rev. **52**(2), 100–106 (2008).
[34]T. Seeholzer, D. Tarau, L. Hollendonner, A. Auer, R. Rachel, D. Grohmann, F. J. Giessibl, and A. J. Weymouth, "A next-generation qPlus-sensor-based AFM setup: Resolving archaeal S-layer protein structures in air and liquid," J. Phys. Chem. B **127**, 6949–6957 (2023).
[35]Y. Yamada, T. Ichii, T. Utsunomiya, K. Kimura, K. Kobayashi, H. Yamada, and H. Sugimura, "Fundamental and higher eigenmodes of qPlus sensors with a long probe for vertical-lateral bimodal atomic force microscopy," Nanoscale Adv. **5**(3), 840–850 (2023).
[36]M. D. M. Dryden and A. R. Wheeler, "DStat: A versatile, open-source potentiostat for electroanalysis and integration," PLoS One **10**(10), e0140349 (2015).
[37]T. Utsunomiya, Y. Yokota, T. Enoki, and K. I. Fukui, "Potential-dependent hydration structures at aqueous solution/graphite interfaces by electrochemical frequency modulation atomic force microscopy," Chem. Commun. **50**(98), 15537–15540 (2014).
[38]M. Müllner, *Oxides in Aqueous Solution: Stability and Activity at the Atomic Scale* (Technical University, Vienna, 2021).
[39]D. Tománek, S. G. Louie, H. J. Mamin, D. W. Abraham, R. E. Thomson, E. Ganz, and J. Clarke, "Theory and observation of highly asymmetric atomic structure in scanning-tunneling-microscopy images of graphite," Phys. Rev. B **35**(14), 7790–7793 (1987).
[40]I. P. Batra, N. García, H. Rohrer, H. Salemink, E. Stoll, and S. Ciraci, "A study of graphite surface with stm and electronic structure calculations," Surf. Sci. Lett. **181**(1–2), 126–138 (1987).
[41]S. Hembacher, F. J. Giessibl, J. Mannhart, and C. F. Quate, "Revealing the hidden atom in graphite by low-temperature atomic force microscopy," Proc. Natl. Acad. Sci. U. S. A. **100**(22), 12539–12542 (2003).
[42]D. Martin-Jimenez, E. Chacon, P. Tarazona, and R. Garcia, "Atomically resolved three-dimensional structures of electrolyte aqueous solutions near a solid surface," Nat. Commun. **7**(1), 12164 (2016).
[43]K. Suzuki, N. Oyabu, K. Kobayashi, K. Matsushige, and H. Yamada, "Atomic-resolution imaging of graphite-water interface by frequency modulation atomic force microscopy," Appl. Phys. Express **4**(12), 125102 (2011).
[44]H. Söngen, Y. Morais Jaques, L. Zivanovic, S. Seibert, R. Bechstein, P. Spijker, H. Onishi, A. S. Foster, and A. Kühnle, "Hydration layers at the graphite-water interface: Attraction or confinement," Phys. Rev. B **100**(20), 205410 (2019).